Soft Matter

Accepted Manuscript

ROYAL SOCIETY OF CHEMISTRY

www.rsc.org/softmatter

Flow-induced alignment of (100) fcc thin film colloidal crystals

Midhun Joy, Tanyakorn Muangnapoh, Mark A. Snyder, and James F. Gilchrist**

Department of Chemical and Biomolecular Engineering, Lehigh University, Bethlehem, PA, USA

E-mail: gilchrist@lehigh.edu, Tel: +1 610 758 4781;
snyder@lehigh.edu, Tel: +1 610 758 6834; Fax: +1 610 758 5057

Table of contents entry

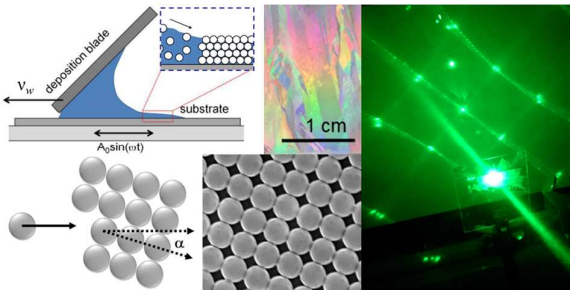

Extensive multi-layer single-crystalline (100) fcc domains covering nearly 40% of a colloidal crystalline film partially oriented relative to the direction of deposition are realized by vibration-assisted convective deposition.

Abstract

The realization of structural diversity in colloidal crystals obtained by self-assembly techniques remains constrained by thermodynamic considerations and current limits on our ability to alter structure over large scales using imposed fields and confinement. In this work, a convective-based procedure to fabricate multi-layer colloidal crystal films with extensive square-like symmetry is enabled by periodic substrate motion imposed during the continuous assembly. The formation of film-spanning domains of (100) fcc symmetry as a result of added vibration is robust across a range of micron-scale monosized spherical colloidal suspensions (e.g., polystyrene, silica) as well as substrate surface chemistries (e.g., hydrophobic, hydrophilic). The generation of extensive single crystalline (100) fcc domains as large as 15 mm^2 and covering nearly 40 % of the colloidal crystalline film is possible by simply tuning coating conditions and multi-layer film thickness. Preferential orientation of the square-packed domains with respect to the direction of deposition is attributed to domain generation based upon a shear-related mechanism. Visualization during assembly gives clues toward the mechanism of this flow-driven self-assembly method.

Introduction

Interest in colloidal crystallization has long been the focus of fundamental studies wherein thermodynamic and kinetic analogies are commonly drawn to atomic systems[1]. In contrast to equilibrium molecular particle assembly[2] dominated by intermolecular and interparticle forces,[3,4] nonequilibrium colloidal self-assembly[5] can be efficiently tailored through modulation of gravitational[6], shear[7–9], as well as electromagnetic[10,11] fields. Among non-equilibrium techniques, convective assembly of colloidal particles[12–15] enables realization of colloidal crystal films with fine control over film thickness (i.e., mono- to multi-layer) and extensive order (i.e., colloidal crystallinity) spanning scales of square millimeters or larger by exploiting evaporation-driven flow in a thin film.

Unique photonic[16–18], magnetic[19,20], and structural[21] applications are reliant, however, upon realization of colloidal assemblies with non-hexagonal packing symmetries oriented parallel to the underlying substrate for achievement or enhancement of specific physical properties. Yet the larger free energy of these structures relative to hexagonally symmetric and face centered cubic close-packed structures, hcp and fcc, respectively, makes them challenging to realize without imposition of external fields or epitaxial fabrication utilizing complex boundary templating. Although non-close packed colloidal phases (e.g, bcc) have been observed in addition to hexagonally close packed (hcp) phases for specific particle volume fractions and charge screening in concentrated suspensions of charge stabilized particles[22], extraction of these assemblies from solution tends to eliminate bcc packing favoring close-packed symmetries. Primarily colloidal crystals with hexagonally symmetric packing in all constituent layers parallel to the substrate upon which they are asembled[6–8,12–15] result. Since hcp and face-centered cubic (fcc) structures differ negligibly (0.005 RT/mole)[23] in their corresponding free energies, the resulting colloidal crystals tend to be

comprised of coexisting hcp and fcc phases. Here, we refer to this mixture of hexagonal symmetries as "random hexagonally close packed" or rhcp arrangements.

The cubic particle symmetry desired for various applications is the same as that which is presented by the (100) facet of an fcc crystal. The spontaneous formation of square-packed colloidal domains by particle self-assembly, the (100) facets of fcc crystals, has been reported at boundaries marking the transition between adjacent hexagonally-packed domains of different multi-layer thickness[12,13,24,25]. Yet, the localization of such faceting to transition regions precludes its scalability to areas greater than several particle diameters. Only particle assembly performed under highly controlled growth conditions on pre-patterned substrates reproducibly yields structures with (100) fcc oriented colloidal-crystal planes. These substrate-patterning approaches[26–33], referred to as colloidal epitaxy,[26] have exploited template morphologies including arrays of square gratings[26–29], pillars[30,31] and square or rectangular inverse pyramidal V-shaped grooves[32]. Because these templating procedures require precise control of the pitch and the diameter of fabricated template features with respect to the colloidal-particle size[28], the achievable extent of the epitaxially grown (100) fcc domains over the predominant (111) fcc oriented packing being generated in the neighboring, unpatterned regions[31] is severely limited.

In this work, we report the discovery of extensive and tunable square-packing (i.e., (100) fcc facets oriented parallel to the underlying substrate) in self-assembled colloidal structures realized simply by the introduction of external oscillatory motion of the substrate during convective assembly of multilayer colloidal crystals. This substrate motion alters flow-patterns of the colloidal particles confined within the liquid film during convective assembly. Besides forming large (100) fcc crystalline domains with relatively few defects, the process also results in colloidal crystals having negligible variation in thickness while simultaneously yielding controlled proportions of both hexagonal and square-packed arrangements.

Results & Discussion

Figure 1 shows a direct comparison between representative multi-layered polystyrene colloidal crystals prepared on glass substrates by blade-based convective deposition methods with (Figure 1e-h) and without (Figure 1a-d) lateral oscillation of the substrate. White light irradiation (Figure 1a,e) of each colloidal crystal reveals iridescent reflections indicative of polycrystallinity, but with marked differences in the corresponding extent of the single crystalline sub-domains. Specifically, vibration-mediated assembly appears to dramatically increase the size of the constituent single crystal domains to extensive mm and even cm scales (Figure 1e). Laser diffraction through these glass-supported samples, carried out using a 532 nm wavelength laser with a 15 mm^2 spot size, confirms the millimeter-scale of the single crystalline domains (i.e., containing more than 10^7 particles with similar packing arrangement and orientation) achieved through vibration-mediated convectie assembly (Figure 1f,g). In contrast, Figure 1b shows the characteristic ringed diffraction pattern from polycrystalline colloidal crystals assembled by conventional (i.e., vibration-free) convective deposition, deriving from lattice mismatch of smaller grains of near exclusive hexagonal symmetry[6–8,12–15] as shown in more detail in the scanning elctron microsocpy (SEM) images in Figure 1c,d.

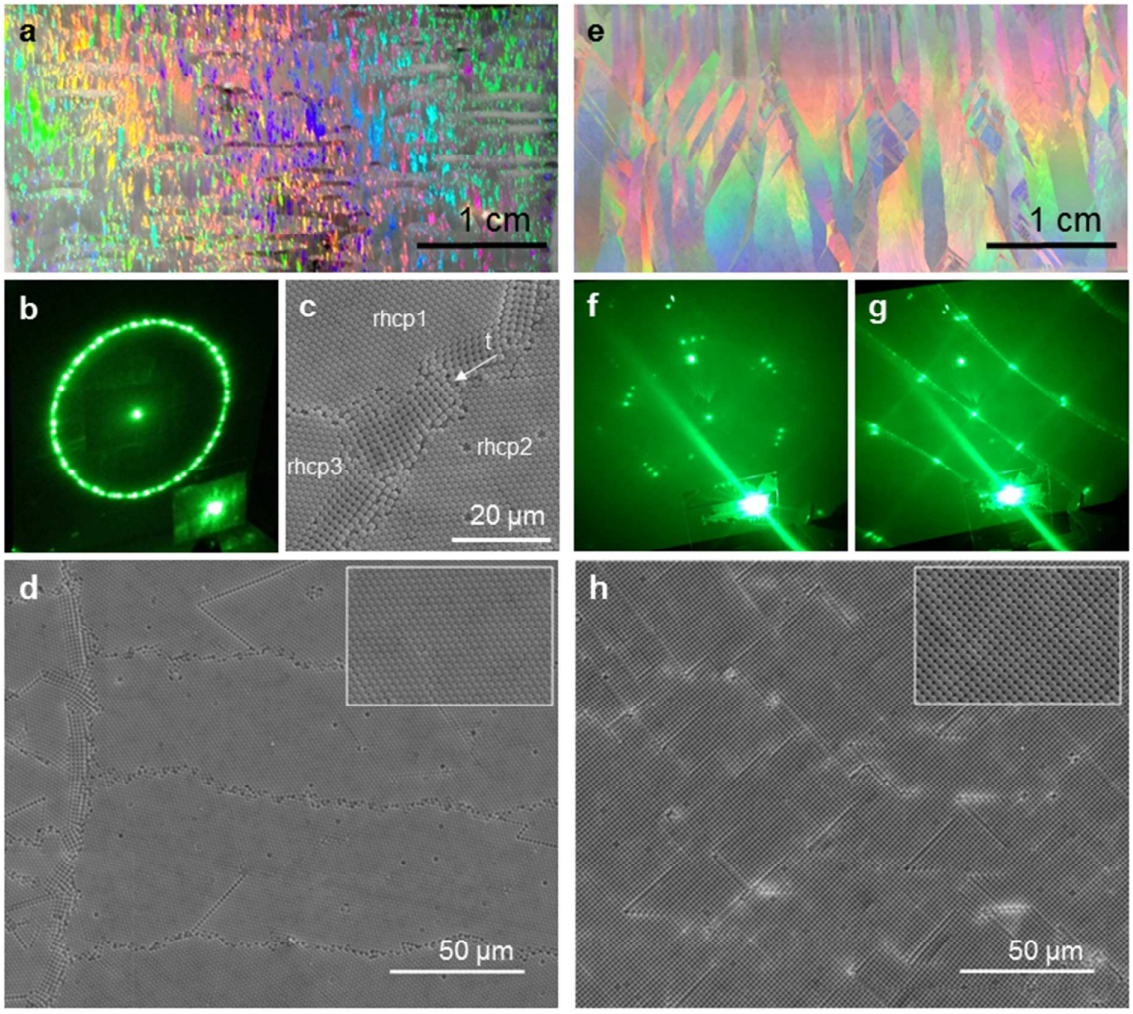

Figure 1. Comparison of colloidal-crystals assembled by conventional (a-d) and vibration-mediated (e-h) convective deposition Images (a,e) show white light irradiation of representative colloidal crystals comprised of 1.5 μm polystyrene particles on glass substrates, revealing differences in polycrystallinity. Laser diffraction of these samples using a 15 mm^2 beam show a polycrystalline region (b) and large individual rhcp (f) and fcc 100 domains (g). The corresponding SEM images of the rhcp colloidal crystal surface (c,d), indicate the micron-scale lattice-mismatched domains of rhcp symmetry. The localized transition ('t' in (c)) are the only regions of square/cubic symmetry in the case of conventionally assembled colloidal crystals, as compared to the mm-scale domains of both hexagonal (f) and square/cubic symmetries (g,h) under vibration-mediated assembly. SEM insets show magnified views of the respective rhcp and square/cubic symmetries.

Laser diffraction from samples assembled by vibration-mediated methods reveals a surpising co-existence of domains with two distinct crystalline symmetries. In addition to crystalline domains of hexagonal symmetry (diffraction with 60^o angular spacing, Figure 1f), commonly observed in colloidal crystals assembled by conventional methods (Figure 1c,d),

domains yielding diffraction patterns with angular spacing of 90^o (Figure 1g) are also observed. Taken together with the large laser spot size, the latter indicates the existence of extensive crystalline domains of square/cubic symmetry (e.g., fcc (100) or square-packed domains) as shown in the SEM image in Figure 1h, the formation of which has not previously been reported without reliance on external fields, complex and multi-step epitaxial growth, or as highly localized artefacts of only a few particle diameters arising at points of transition between hexagonally symmetric grains of different multi-layer thickness (e.g., region '*t*', Figure 1c).

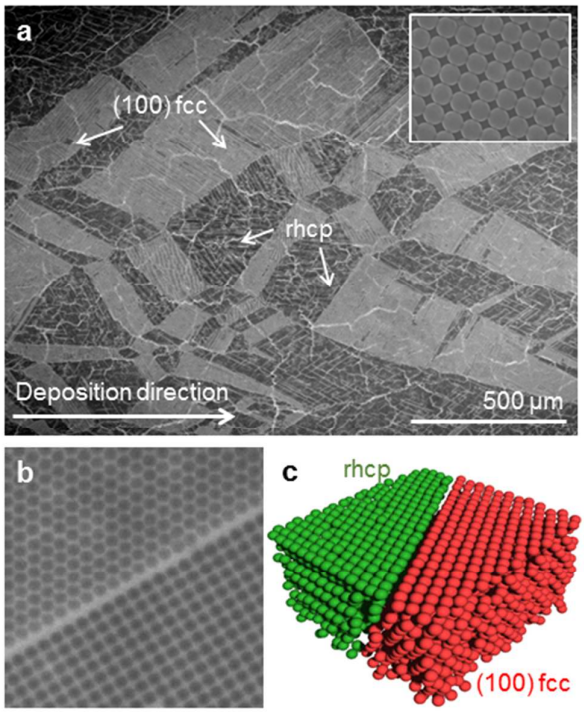

Figure 2. Structural analysis of multi-layer cubic colloidal-crystals achieved by vibration-assisted convective assembly carried out by (a) SEM analysis of the top surface of the colloidal crystal (square packing of '(100) fcc' domains shown in inset), (b) CLSM imaging of adjacent single crystalline domains at the crystal-substrate interface, and (c) 3D reconstruction of the colloidal crystalline structure at a representative grain boundary. Analysis is shown for representative assemblies of 0.93 µm polystyrene (PS) particles.

The coexistence of domains of rhcp and square/cubic symmetry is further explored in **Figure 2**a, where a lower magnification SEM image of the top surface of a representative colloidal crystal obtained by vibration-assisted convective deposition of 0.93 µm polystyrene

(PS) particles reveals domains with distinct variation in brightness corresponding to two distinct colloidal crystalline arrangements at the surface. Whereas darker regions possess a hexagonal arrangement of particles corresponding to the (111) plane of the close-packed structure (rhcp) (Supplementary figure S1 and S2), a square-arrangement of particles is observed at the surface of brighter regions, as shown in the inset to Figure 2a. Complemented by the laser diffraction analysis (Figure 1f,g), which indicates the persistence of such structures throughout the thickness of the colloidal crystal, and the contact between all adjacent particles, the square packing of particles at the surface of these domains is consistent with the structural symmetry associated with the (100) facet of an fcc crystal (Supplementary Figure S3,S4 and S5).

Beyond the laser diffraction experiments, quantification of the bulk crystallinity was carried out by confocal laser scanning microscopy (CLSM) (Figure 2b), a technique enabling collection of optical slices through the thickness of the colloidal crystal and its subsequent 3D-reconstruction (Figure 2c). Whereas the SEM image shown in Figure 2a was collected at the top surface of the colloidal crystal, Figure 2b shows a representative optical slice of adjacent single crystalline domains collected at a focal plane positioned at the interface between the colloidal crystal and the underlying substrate. The confocal image clearly shows the two distinct particle arrangements in the adjacent single crystalline domains consistent with the rhcp and (100) fcc symmetries observed at the surface.

3D rendering of the corresponding series of confocal images spanning the thickness of the colloidal crystal is shown in Figure 2c, with analysis of particle positions confirming the hexagonal and (100) fcc crystal symmetries (see supplemental information). The transition between the adjacent (100) fcc and rhcp domains appears to occur along a sharp, well-defined grain boundary (Figure 2c) extending vertically through the thickness of the crystal (i.e., perpendicular to the underlying substrate and crystal surface). The vertical orientation of the grain boundary, consistent with almost all such measured boundaries in the colloidal crystals

prepared in this study by the vibration-assisted convective deposition approach, lies in clear contrast to epitaxial (100) fcc assemblies reported previously[26–33]. While most grain boundaries have this registry, others occur along incoherent directions with some disorder between phases. In the case of epitaxial assemblies, the generation of square-packed regions progresses similar to a pyramidal structure from the substrate/crystal surface[29] leading to sequential reduction in the effective area of the square-packed surface structure with increasing thickness of the colloidal crystal.

The simultaneous generation of extensive domains of both square and hexagonally packed structures in multi-layer colloidal crystals assembled via vibration-assisted convective deposition stands in striking contrast to other reports on pure rhcp mono- and multi-layer colloidal crystalline structures from vibration-free[12–15] deposition (e.g., Figure 1c,d) and pure hexagonally packed mono-layer colloidal crystals from vibration-assisted approaches[34]. This underscores the apparent sensitivity of the constituent particle symmetry to the vibrations imposed during convective deposition, and the potential additional role of colloidal crystal thickness in controlling the existence, persistence, and extent of the unique (100) fcc domains.

For initial insight into the latter, we have systematically varied the multi-layer thickness of vibration-assisted, convectively deposited colloidal crystals, and have employed extensive CLSM and complementary particle identification and tracking algorithms to quantify properties such as particle-particle connectivity, crystal symmetry, and crystal orientation (see supplementary information for algorithmic details). **Figure 3** depicts how the fraction of square-packed (100) fcc crystalline domains varies with the number of layers in multi-layer colloidal crystal assemblies. Here, the thickness of the colloidal crystal was tuned by controlling either the deposition speed (open symbols, Figure 3) or the evaporative solvent flux (i.e., by relative humidity; filled symbols, Figure 3). The number of layers corresponds to that found in rhcp domains. Both methods of modulating the crystal thickness have been established by previous convective deposition studies[12].

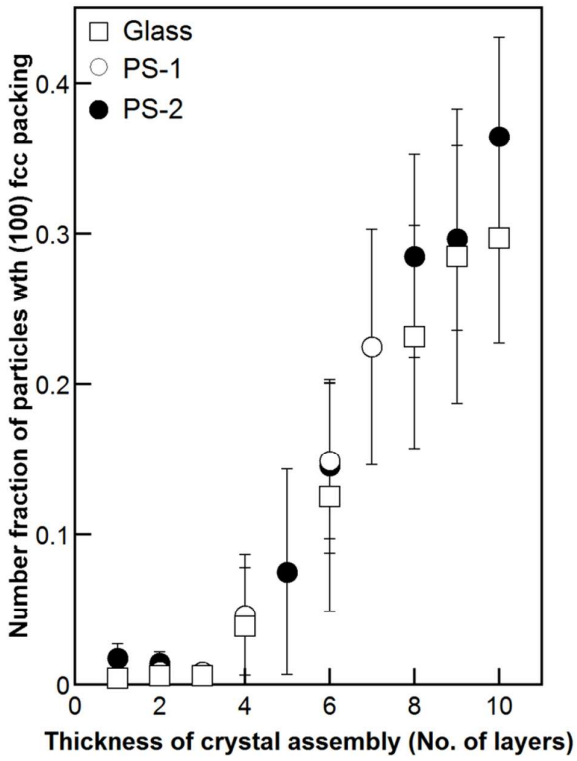

Figure 3. Sensitivity of fraction of (100) fcc domains to colloidal crystal thickness and substrate chemistry Variation of the number fraction of (100) fcc domains with number of layers for colloidal-crystal assemblies of 0.93 μm PS particles, on plain glass (□) where film thickness has been changed by tuning the vibration-assisted convective deposition rate from 2 μm/s (monolayer colloidal crystal) to 6 μm/s (10-layer colloidal crystal) in the presence of a fixed relative humidity of 55 %. Complementary analysis is shown of colloidal crystals deposited on a polystyrene film (circles), for which the thickness of the multi-layered colloidal crystal has been tuned by variation in deposition speed, PS-1 (○), and variation in humidity, PS-2(●)

The fraction of square packing in the crystal assembly increases with increasing crystal thickness after an apparent threshold thickness of approximately 3 layers is exceeded. At or below the threshold thickness, vibration-assisted colloidal crystal assemblies are dominated by hexagonally packed regions with small but measurable fractions of (100) fcc crystal domains. The small fraction of (100) fcc domains are attributed to highly localized regions marking transitions in the number of multi-layers in the colloidal crystal, a phenomenon described previously to result from confinement effects[13] (e.g., Supplementary Figure S6).

As shown in Figure 3, as the threshold colloidal crystal thickness is exceeded, the mechanism responsible for the generation of (100) fcc structures due to vibration becomes increasingly dominant. Colloidal crystals comprised of nearly 40% (100) fcc domains are achieved for samples as thick as just ten layers. The extensive (100) fcc domains appear to form independent of the aforementioned thickness-transition effects[12,13,24,25]. CLSM analysis at grain boundaries in the colloidal crystal (e.g., Figure 2c) has confirmed that square-packed domains generally have identical numbers of particle layers as bordering hexagonally-packed regions such that the colloidal crystals have a remarkably uniform overall thickness with variations between domains differing only by the concomitant lattice parameter differences between (100) and (111) planes.

Perhaps as noteworthy as the facile formation and extent of the (100) fcc domains is the apparent robustness of the process to a wide range of system conditions and material properties. Figure 3 shows remarkably good agreement for the threshold number of colloidal layers (i.e., ca. 3) and the measured fraction of (100) fcc domains with increasing thickness for crystals for which the thickness was tuned by different means (i.e., deposition rate, evaporative flux). Furthermore, the monotonically increasing fraction of (100) fcc regions appears insensitive to variations in chemical composition of the substrate. Similar results were obtained for assemblies of PS particles on glass as well as glass-supported 2 μm polystyrene films. Finally, large (100) fcc domains were similarly obtained for particles ranging in size from ca. 500 nm to 1.5 μm and spanning function to include charged- or sterically-stabilized particles (Supplementary Figure S7).

Ultimately, the realization of flow-induced (100) fcc domains by vibration-assisted convective deposition may eliminate the need for accurate substrate patterning and highly-controlled crystal growth that is critical for achieving colloidal crystals of similar crystalline symmetry by alternative state-of-the-art colloidal epitaxy approaches[26–33]. The robustness of the process coupled with the intrinsic scalability of convective deposition holds exciting

potential for realization of large area (100) fcc crystals. The ease with which the colloidal crystal films can be delaminated from the substrate upon which they were deposited for the purpose of generating free standing structures also circumvents one of the key limitations of epitaxial grown structures for which such delamination is more difficult. Yet, scalability hinges, at least in part, upon the ability to tune properties such as the size and orientation of the (100) fcc domains, a prospect demanding fundamental insight into the underlying mechanisms of their formation (e.g., nucleation, growth), and their sensitivities to system parameters and flow conditions intrinsic to vibration-assisted convective deposition.

We have carried out CLSM and subsequent image analysis (see supplemental information) in order to fully quantify the size and distribution of the (100) fcc crystalline domains and surrounding rhcp domains as well as to assess whether the domains are preferentially oriented. Whereas, laser diffraction experiments (Figure 1f,g) suggest that some crystalline domains are as large as several millimeters, CLSM at a resolution enabling accurate determination of single particle locations is limited to analysis only of sequential regions containing ca. 4500 particles. Owing to inaccuracies associated with the correlation of particle locations across neighboring frames, we have carried out CLSM-based calculations of domain size and domain orientation by treating each confocal frame as a separate entity.

Figure 4a-d shows four representative confocal scans with various specified fractions of (100) fcc crystalline domains, that have been further parsed according to their relative size based upon the number, *n*, of particles contained within each. Figure 4e shows a rendered image obtained by combining several consecutive confocal frames along the direction of deposition. In addition to underscoring the extent of the (100) fcc crystalline domains, Figure 4e also reveals an orientation of the large (100) fcc crystalline domain analyzed therein of $\alpha=30^{o}$ relative to the direction of deposition. For reference, the orientation of domains of various sizes is also specified in Figure 4a-e.

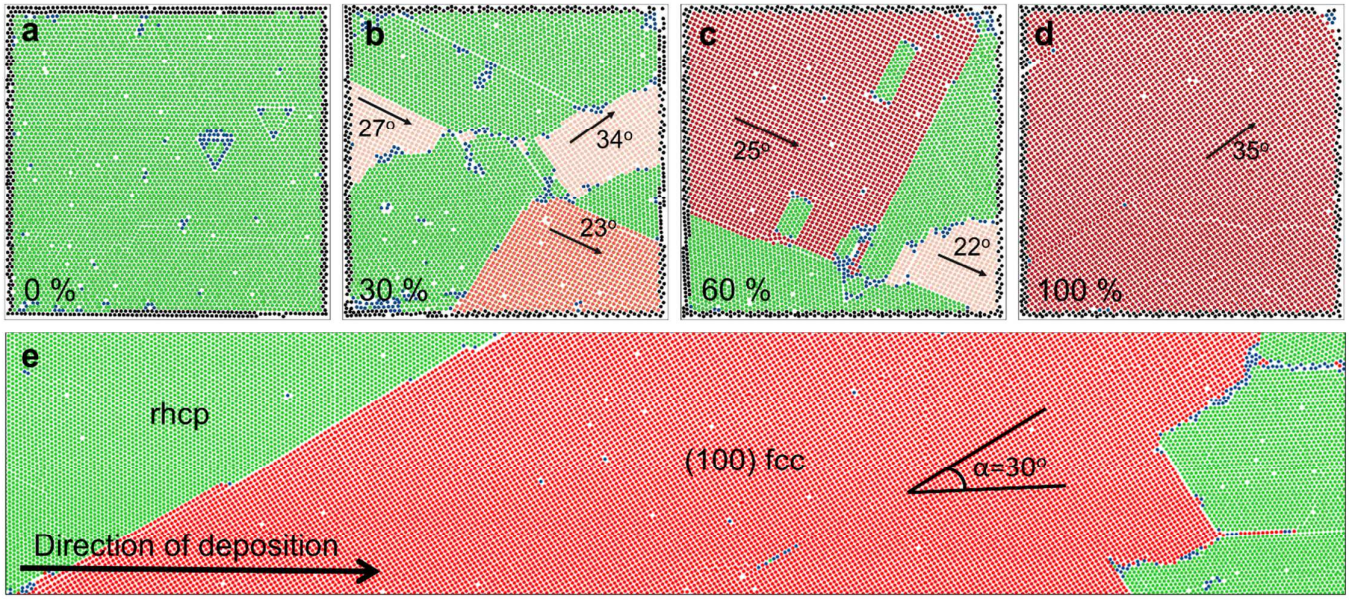

Figure 4. Quantitative CLSM-based analysis of (100) fcc fraction, domain size, orientation Panels (a-d) depict the result of image analysis including identification of crystal symmetry (e.g., rhcp - green, (100) fcc – light red to dark red as a function of domain size), number fraction of (100) fcc (% specified), domain size (based on number, *n*, of constituent particles: small, n < 1500 particles; medium, 1500 ≤ n ≤ 3000; large, n >3000), and domain orientation, α, relative to the direction of deposition (e) Panoramic view of a representative extensive (100) fcc domain obtained by combining multiple sequential confocal images of the colloidal crystal along the direction of deposition.

The result of more extensive analysis beyond the snapshots shown in Figure 4 of the size, distribution, and orientation of (100) fcc domains within vibration-assembled colloidal

crystals of various multi-layer thickness, N, is shown in **Figure 5**. To help facilitate analysis, the (100) fcc domains were categorized into bins of relative sizes ranging from (1) those having less than 1500 particles on the surface, or roughly one third of the image size, to (3) crystals covering the majority of the image and clearly spanning beyond it. The probabilities of (100) fcc domains of various sizes are shown in the left column. While small domains ($n<1500$ particles) exist in the thinnest ($N = 3$ multi-layers) to the thickest ($N=9$ multi-layers) colloidal crystals, the distribution of fcc (100) domain size shifts dramatically from small to large with increasing colloidal crystal thickness. For relatively thin colloidal crystals having $N = 3$ layers, square-packed structures exist entirely as small domains. These domains arise at regions of transition between grains for changes in thickness as has been reported previously[24]. As the overall colloidal crystal thickness increases to $N \geq 5$, the fraction of such small domains becomes insignificant, with the majority associated with the edges of larger domains (i.e., identified as small domains in Figure 4b,c). This is accompanied by a shift toward larger square-packed domains that extend across multiple CLSM images.

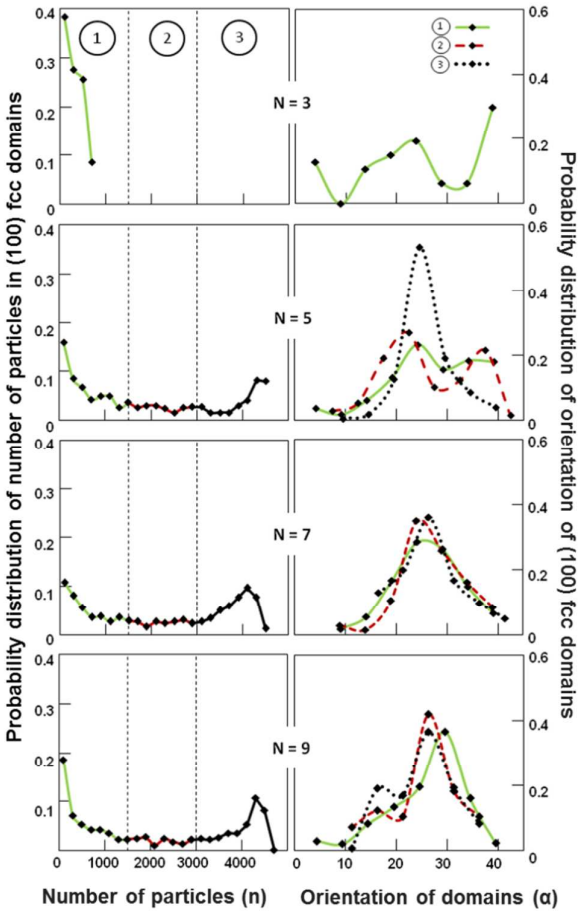

Figure 5. Probability of (100) fcc domain size, orientation Probability of domain size in terms of number of particles, *n*, (left column) and corresponding domain orientation, α, (right column) for multi-layer colloidal crystals comprised of specified numbers of layers, N. Line style is used to denote domain size according to number, *n*, of particles included: (1) solid (small, n < 1500 particles), (2) dashed (medium, 1500 ≤ n ≤ 3000), and (3) dotted (large, n>3000).

The orientation, α, of the (100) fcc domains in relation to the direction of deposition is likewise sensitive to the number of particle layers comprising the colloidal crystal. The smallest domains found for colloidal crystals comprised of N = 3 particle layers have no clear orientation, only weakly favoring 20º < α < 30º. Small and medium-sized (100) fcc domains found in samples assembled into N = 5 layers also have no clear orientation, however, they are more strongly aligned at an angle α = 25º relative to the assembly direction. For colloidal crystal of N ≥ 7 particle layers, a clear preferential alignment of the (100) fcc along 25º ≤ α ≤

30º is observed, with the smaller and medium-sized domains drawing alignment through association with larger domains not visualized in their entirety. The reduction in the standard deviation associated with domain orientation as the domains become larger corresponds to the overall tendency of the domains to be aligned at ~ 30º in the colloidal crystal assembly obtained through vibration-assisted convective deposition. In samples that are predominantly rhcp, there is no correlation in the crystal lattice with regard to the deposition direction, nor has it been reported previously in non-epitaxial convective deposition. Regions of rhcp neighboring fcc domains have preferred orientation, perhaps as a result of lateral templating from the fcc regions.

This observation of aligned fcc (100) domains supports the development of a hypothesis where the underlying mechanism is related to the meniscus and suspension flow characteristics regulated by the addition of vibration to the convective deposition process. It is apparent that the mechanism for colloidal assembly in vibration-assisted convective deposition differs significantly from conventional (i.e., vibration-free) convective assembly. Conventional convective assembly procedures for multilayer synthesis having a static meniscus which remains unaltered in shape throughout the process wherein particles assemble predominantly by convective steering[35,36] . Previous studies have suggested the optimal growth front is a (311) fcc plane[35] oriented at an angle of 100º based on the assumption that the free surface has hexagonal symmetry.

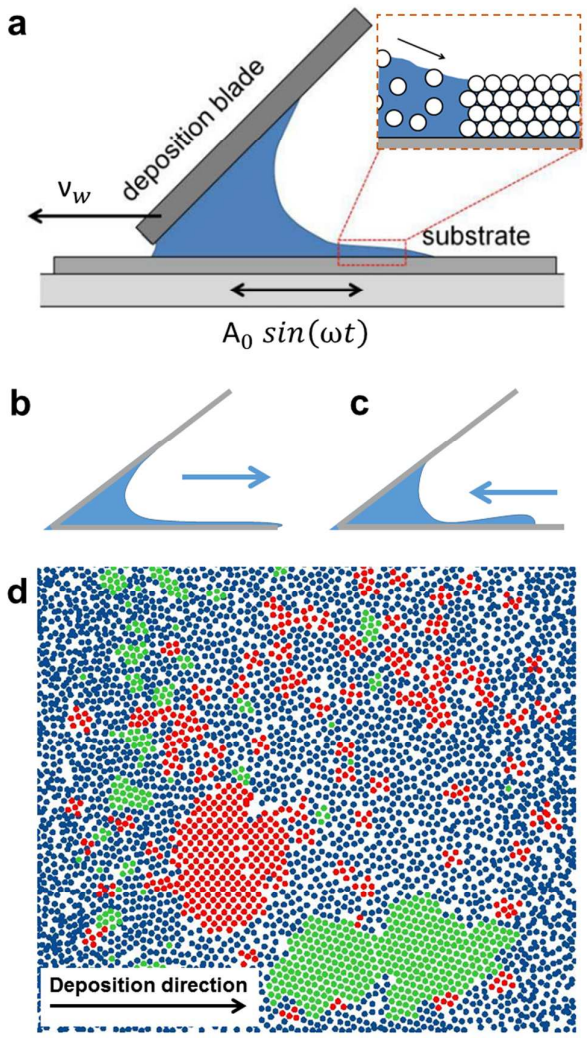

Figure 6. Schematic of vibration-assisted convective assembly and image analysis of in situ structure during assembly. (a) Schematic of the experimental setup for the vibration-assisted convective assembly procedure wherein the deposition blade is advanced at a velocity, v_w, while the substrate undergoes oscillatory in-plane vibrations, $A_0\sin(\omega t)$, leading to periodic (b) elongation and (c) compression of the liquid meniscus during each cycle of the vibration. (d) Simultaneous formation of square and hexagonally packed regions through a nucleation-growth mechanism demonstrated by a color-rendered in-situ confocal image. The image obtained using 0.93 µm PS particles and at 40 Hz and amplitude of ~10 µm, comprises of both hexagonal (green) and square (red) packed nucleates being generated in the suspension (blue), suggesting a nucleation-growth mechanism during convective assembly.

This mechanism, however, cannot be extended for the vibration-assisted process. The addition of external periodic vibration creates a back-and-forth movement of the meniscus, resulting in a dynamic meniscus shape, as depicted in **Figure 6**b,c. One possible mechanism for the distinct formation of (100) fcc crystalline domains in this process could be that the

resulting shearing of charge-stabilized particle suspensions assists colloidal assembly into structures other than rhcp symmetries. This has been investigated in many other non-equilibrium experimental studies of simple sheared colloidal systems[37–40] as well as order induced by flow in Couette devices[41] as well as planar geometries[42] and Poiseuille flow[43]. When a metastable particle aggregate in a suspension undergoes oscillatory shear, the resulting structure depends on the direction of shear forces as well as the relative magnitudes of shear and inter-particle forces[44–46]. At low particle concentration and high shear rates, shear can result in coordinated string-like movement of particles[42]. In all of these systems, the flow streamlines are unidirectional and constrained within the solid boundaries, and results predominantly in particle-clusters with hexagonal symmetry parallel to the boundaries of the system. However in the case of the vibration-assisted procedure outlined in this work, the dynamic meniscus shape arising from its periodic sinusoidal translation generates multi-directional flow streamlines within the thin film region, which has the potential to affect the relative lattice positions of individual particles in the clusters. This results in the simultaneous generation of clusters with both hexagonal and square symmetry, which act as nucleates for the addition of incoming particles and can be observed in Figure 6d.

Alternatively, another explanation of the generation of colloidal crystals with a combination of hexagonal and square-packing arrangement of the constituent particles having alignment with respect to the direction of deposition can consider the preferential growth of randomly oriented colloidal nucleates. As the suspension is concentrated as it approaches the thin film region, it crosses the liquid-crystal coexistence concentration, either that found in equilibrium systems or at a concentration where crystallization is assisted by the imposed shear from vibration. These fcc nucleates, having random orientation, grow in directions relative to the deposition direction. Those having their (100) plane aligned with the substrate grow without disrupting their lattice arrangement at a comparable or faster rate than nucleates having other orientations. This can be observed in Figure 5 and 6d in which the large (100)

fcc domains have a preferential orientation of 30^{o} with respect to the deposition direction. Moreover, although numerous square-packed (red) nucleates can be observed in Figure 6d, we speculate that those domains which can grow need to possess a preferential orientation with respect to the incoming particles.

In select experiments performed on the CLSM enabling *in situ* scanning during assembly, evidence of this mechanism is suggested by coexistence of rhcp and fcc (100) substrate-aligned nucleates in the region just upstream of the final arrested polycrystalline colloidal assembly (Figure 6d). While only heuristics can be derived through this experiment, the evidence motivates further studies into nucleation and preferential growth that may favor coupling of crystalline microstructure and convection direction toward assembly of a polycrystalline thin film leading to large flow- and substrate-aligned fcc crystalline domains. Perhaps only studies allowing experimental particle tracking during vibration-assisted convective assembly or multiscale time-resolved simulations that track both the particle phase and the dynamic motion of the interface can give further insight into the mechanism of assembly.

Experimental Section

Vibration assisted convective deposition was employed to assemble particles from aqueous solutions into multi-layer colloidal crystal films. The experimental setup described previously[34] employs a glass microscope slide as a coating blade, fixed at an angle of 45^{o} and ~1 mm above an underlying substrate. The bottom edge of the blade was made hydrophobic through attachment of Parafilm so as to confine small volumes (200 µl) of colloidal solutions in the angle between the blade and substrate. Continuous convective deposition of colloidal crystalline films was achieved by particle convection to and pinning at the contact line of the meniscus with the substrate during translation of the latter. In addition to linear translation of the substrate, characteristic of conventional convective deposition processes[13], colloidal

crystalline depositions in this work were carried out with the addition of controlled in-plane vibrations imposed in the same direction as that of the meniscus withdrawal. This was achieved through combination of a linear mechanical driver (kdScientific) and a mechanical driver (PASCO SF-9324) coupled with a waveform sinusoidal signal generator (Agilent 33220A).

Colloidal crystalline films were prepared in an enclosed chamber under controlled temperature (nominally 24 ^{o}C) and humidity conditions (nominally 20%, but systematically varied from 4% to 90%). Nominal depositions were prepared from a 10% w/w suspension of 0.93 μm or 1.5 μm polystyrene (PS; Thermo-scientific) or silica particles (Fiber Optic Center Inc.) in water on 45 mm x 50 mm microscope cover-glass (Fisherbrand) or glass-supported PS substrates. The latter was prepared by convective deposition of 0.30 μm PS particles (10 % w/w) into ca. 2 μm films (14 μm/s at a humidity of 20%) followed by melting at 240 ^{o}C for 45 min. In all cases, glass substrates were pre-treated with piranha solution and subsequently rinsed with distilled water and dried prior to deposition. Colloidal crystalline film thickness, N, was tuned by controlling the rate of linear translation of the substrate, v_w (2–10 μm/s), and relative humidity (i.e., evaporative solvent flux, j_e) according to the equation (1) proposed by Dimitrov and Nagayama[12]

$$N = \frac{\beta l}{0.605}\frac{j_e \varphi}{v_w d(1-\varphi)} \qquad (1)$$

where βl is a constant, φ is the suspension concentration and d is the diameter of particles in the suspension.. Nominal waveform generation, $A_0 sin(\omega t)$, was carried out at a frequency of ω = 40 Hz and amplitude of ca. A_0 = 1200 μm.

Colloidal crystalline films were analyzed using white light irradiation and scanning-electron microscopy (SEM) on a Hitachi 4300 instrument to assess particle packing at the top-most layer of the film, and by laser scattering (λ = 532 nm, 15 mm^2 spot size) by the films supported on glass substrates for insight into the bulk crystallinity and crystal symmetry. The

colloidal crystal samples were also analyzed using laser scanning confocal microscopy (CLCM, Visitech) after wetting samples with 8 mM Rhodamine-B dye in DMSO. CLSM scans were taken at sequential axial positions along the direction of coating as well as through the thickness of the colloidal crystal film. Confocal images were processed using IDL to identify the individual particle locations[47,48] in the crystal assembly, and, subsequently, the number of particle layers comprising the colloidal crystalline film, the local crystal symmetry (e.g., hexagonally close packed, hcp; face centered cubic, fcc; mixtures thereof defined here as random hexagonally close packed, rhcp), the size of single-crystalline domains, the number fraction of the sample bearing a specified crystal symmetry, and the crystal domain orientation (α) relative to the coating direction.

Conclusion

The self-arrangement of colloidal particles into non-hexagonal arrangement under the influence of flow fields has been suggested as a viable alternative to epitaxial approaches to engineer the packing structure in colloidal crystals. This approach adds vibration to the convective deposition process, inducing variations in solvent flow characteristics and meniscus properties, thereby resulting in spontaneous arrangement of particles in an oriented fcc (100) pattern parallel to the substrate and at a preferential angle $25^{o} \leq \alpha \leq 30^{o}$ relative to the mean flow direction. This spontaneous ordering has been achieved in the absence of thickness variations, with an increasing trend for the phenomena observed with an increase in the number of layers of the colloidal crystal assembly. The possibility that variations of flow characteristics can organize the particles into various packing arrangements opens up new avenues to obtain tailored crystal structures tuned to the desired optical and structural requirements.

Supporting Information
Supporting Information is available online.

Acknowledgements

Data analysis was performed using code developed by Crocker and Grier using the tutorial and additional algorithms provided by Professor Eric Weeks[48]. We acknowledge funding from the NSF Scalable Nanomanufacturing Program under grant No. 1120399.

Received: ((will be filled in by the editorial staff))
Revised: ((will be filled in by the editorial staff))
Published online: ((will be filled in by the editorial staff))

References

[1] P. N. Pusey, W. van Megen, *Nature* **1986**, *320*, 340.

[2] D. Philp, J. F. Stoddart, *Angew. Chemie* **1996**, *35*, 1154.

[3] Y. Min, M. Akbulut, K. Kristiansen, Y. Golan, J. Israelachvili, *Nat. Mater.* **2008**, *7*, 527.

[4] K. J. M. Bishop, C. E. Wilmer, S. Soh, B. A. Grzybowski, *Small* **2009**, *5*, 1600.

[5] G. M. Whitesides, B. Grzybowski, *Science.* **2002**, *295*, 2418.

[6] S. H. Park, D. Qin, Y. Xia, *Adv. Mater.* **1998**, *10*, 1028.

[7] P. Jiang, M. J. McFarland, *J. Am. Chem. Soc.* **2004**, *126*, 13778.

[8] T. Ruhl, P. Spahn, G. P. Hellmann, *Polymer.* **2003**, *44*, 7625.

[9] L. T. Shereda, R. G. Larson, M. J. Solomon, *Phys. Rev. Lett.* **2010**, *105*, 228302.

[10] R. C. Hayward, D. A. Saville, I. A. Aksay, *Nature* **2000**, *404*, 56.

[11] S. K. Smoukov, S. Gangwal, M. Marquez, O. D. Velev, *Soft Matter* **2009**, *5*, 1285.

[12] A. Dimitrov, K. Nagayama, *Langmuir* **1996**, *12*, 1303.

[13] B. G. Prevo, O. D. Velev, *Langmuir* **2004**, *20*, 2099.

[14] M. Ghosh, F. Fan, K. J. Stebe, *Langmuir* **2007**, *23*, 2180.

[15] P. Kumnorkaew, Y. K. Ee, N. Tansu, J. F. Gilchrist, *Langmuir* **2008**, *24*, 12150.

[16] Y. A. Vlasov, X. Z. Bo, J. C. Sturm, D. J. Norris, *Nature* **2001**, *414*, 289.

[17] C. Jin, Z. Y. Li, M. A. McLachlan, D. W. McComb, R. M. De La Rue, N. P. Johnson, *J. Appl. Phys.* **2006**, *99*, 116109.

[18] Z. Yang, X. Huang, S. Li, J. Zhou, *J. Am. Ceram. Soc.* **2009**, *92*, 1596.

[19] S. Sun, C. B. Murray, D. Weller, L. Folks, A. Moser, *Science.* **2000**, *287*, 1989.

[20] O. Kazakova, M. Hanson, P. Blomqvist, R. Wäppling, *Phys. Rev. B* **2004**, *69*, 094408.

[21] X. Z. An, A. B. Yu, *Powder Technol.* **2013**, *248*, 121.

[22] E. B. Sirota, H. D. Ou-Yang, S. K. Sinha, P. M. Chaikin, *Phys. Rev. Lett.* **1989**, *62*, 1524.

[23] L. V. Woodcock, *Nature* **1997**, *385*, 141.

[24] P. Pieranski, L. Strzelecki, B. Pansu, *Phys. Rev. Lett.* **1983**, *50*, 900.

[25] L. Meng, H. Wei, A. Nagel, B. J. Wiley, L. E. Scriven, D. J. Norris, *Nano Lett.* **2006**, *6*, 2249.

[26] A. Van Blaaderen, R. Ruel, P. Wiltzius, *Nature* **1997**, *385*, 321.

[27] J. Zhang, A. Alsayed, K. H. Lin, S. Sanyal, F. Zhang, W.-J. Pao, V. S. K. Balagurusamy, P. A. Heiney, A. G. Yodh, *Appl. Phys. Lett.* **2002**, *81*, 3176.

[28] D. K. Yi, E. M. Seo, D. Y. Kim, *Appl. Phys. Lett.* **2002**, *80*, 225.

[29] W. Lee, A. Chan, M. A. Bevan, J. A. Lewis, P. V. Braun, *Langmuir* **2004**, *20*, 5262.

[30] J. P. Hoogenboom, C. Retif, E. de Bres, M. van de Boer, A. K. van Langen-Suurling, J. Romijn, A. van Blaaderen, *Nano Lett.* **2004**, *4*, 205.

[31] C. Jin, M. A. McLachlan, D. W. McComb, R. M. D. La Rue, N. P. Johnson, *Nano Lett.* **2005**, *5*, 2646.

[32] Y. Yin, Z. Y. Li, Y. Xia, *Langmuir* **2003**, *19*, 622.

[33] M. Tanaka, N. Shimamoto, T. Tanii, I. Ohdomari, H. Nishide, *Sci. Technol. Adv. Mater.* **2006**, *7*, 451.

[34] T. Muangnapoh, A. L. Weldon, J. F. Gilchrist, *Appl. Phys. Lett.* **2013**, *103*, 181603.

[35] D. D. Brewer, J. Allen, M. R. Miller, J. M. de Santos, S. Kumar, D. J. Norris, M. Tsapatsis, L. E. Scriven, *Langmuir* **2008**, *24*, 13683.

[36] P. Born, A. Munoz, C. Cavelius, T. Kraus, *Langmuir* **2012**, *28*, 8300.

[37] W. D. Dozier, P. M. Chaikin, *J. Phys.* **1982**, *43*, 843.

[38] B. J. Ackerson, N. A. Clark, *Physica* **1983**, *118A*, 221.

[39] L. B. Chen, C. F. Zukoski, B. J. Ackerson, H. J. M. Hanley, G. C. Straty, J. Barker, C. J. Glinka, *Phys. Rev. Lett.* **1992**, *69*, 688.

[40] L. Chen, M. Chow, B. Ackerson, C. Zukoski, *Langmuir* **1994**, *36*, 2817.

[41] B. J. Ackerson, *J. Rheol.* **1990**, *34*, 553.

[42] E. J. Stancik, A. L. Hawkinson, J. Vermant, G. G. Fuller, *J. Rheol.* **2004**, *48*, 159.

[43] T. Sawada, Y. Suzuki, A. Toyotama, N. Iyi, *Japan J. Appl. Phys.* **2001**, *40*, L1226.

[44] M. D. Haw, W. C. K. Poon, P. N. Pusey, *Phys. Rev. E* **1998**, *57*, 6859.

[45] P. Panine, T. Narayanan, J. Vermant, J. Mewis, *Phys. Rev. E* **2002**, *66*, 022401.

[46] T. H. Besseling, M. Hermes, A. Fortini, M. Dijkstra, A. Imhof, A. van Blaaderen, *Soft Matter* **2012**, *8*, 6931.

[47] J. C. Crocker, D. G. Grier, *J. Colloid Interface Sci.* **1996**, *310*, 298.

[48] J. C. Crocker, E. R. Weeks, Particle tracking using IDL; http://www.physics.emory.edu/~weeks/idl/.

Table of contents entry

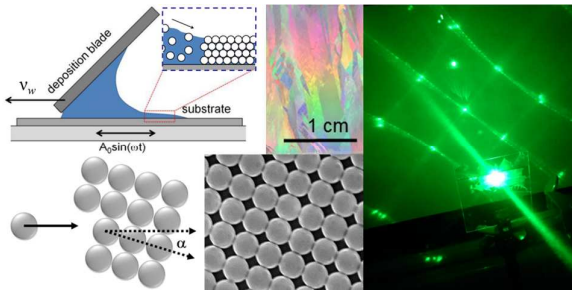

Extensive multi-layer single-crystalline (100) fcc domains covering nearly 40% of a colloidal crystalline film partially oriented relative to the direction of deposition are realized by vibration-assisted convective deposition.